

Communication

CO₂ Adsorption by Bamboo Biochars Obtained via a Salt-Assisted Pyrolysis Route

Xing Xie¹, Mangmang Li¹, Dan Lin¹, Bin Li^{1,2,*} , Chaoen Li³  and Dongjing Liu^{1,*}¹ School of Energy and Power Engineering, Jiangsu University, Zhenjiang 212013, China² School of Engineering, Anhui Agricultural University, Hefei 230036, China³ School of Civil and Transportation Engineering, Ningbo University of Technology, Ningbo 315016, China

* Correspondence: libin198520@126.com (B.L.); liudongjing@ujs.edu.cn (D.L.)

Abstract: Recently, salt-assisted pyrolyzation has been deemed an emerging and efficient method for the preparation of biochars due to its facile operation as well as its good structural and chemical properties. In this work, biochars (MBCx) are prepared by heating bamboo powders in eutectic salts (Li₂CO₃ + K₂CO₃) at 500–600 °C in the air. Multiple technologies are employed to examine the physicochemical properties of bamboo biochars. Correlations between heating temperature and structural features and carbon dioxide uptakes of bamboo biochars have been investigated. The results show that heating temperature has a significant influence on the physicochemical properties of bamboo biochars. With the elevation of the heating temperature, the defect structures of bamboo biochars gradually ascend, especially when the heating temperature reaches 600 °C. MBCx biochars visibly exceed conventional bamboo biochar prepared via pyrolyzation in a nitrogen stream free of salt addition. Pyrolysis of bamboo in eutectic salts endows biochars with higher oxygen content and more carbon defects, which likely accounts for their better CO₂ capture activities.

Keywords: biomass pyrolysis; molten salt; biochar; CO₂ capture; bamboo



Citation: Xie, X.; Li, M.; Lin, D.; Li, B.; Li, C.; Liu, D. CO₂ Adsorption by Bamboo Biochars Obtained via a Salt-Assisted Pyrolysis Route. *Separations* **2024**, *11*, 48. <https://doi.org/10.3390/separations11020048>

Academic Editor: Mohamed Khayet

Received: 17 January 2024

Revised: 1 February 2024

Accepted: 4 February 2024

Published: 6 February 2024



Copyright: © 2024 by the authors. Licensee MDPI, Basel, Switzerland. This article is an open access article distributed under the terms and conditions of the Creative Commons Attribution (CC BY) license (<https://creativecommons.org/licenses/by/4.0/>).

1. Introduction

Greenhouse gas emissions, especially carbon dioxide (CO₂), have overgrown drastically in recent decades, mainly owing to human activities in diverse industrial sectors, leading to severe weather and climate change, such as droughts, floods, global warming, and sea level rise [1]. CO₂ capture and sequestration is regarded as an effective method to eliminate carbon dioxide emissions [2]. So far, aqueous amine scrubbing is the most mature technique for CO₂ removal from gas streams [3]. Nevertheless, the amine absorption process commonly suffers from several drawbacks, for instance, low absorption capacity, poor stability, solvent loss and toxicity, equipment corrosion, and high energy consumption from solvent regeneration [4]. In this regard, the adsorption technique using porous materials seems to be a good replacement for the energy-intensive amine scrubbing process for CO₂ removal [5].

Currently, a host of porous materials, for instance, zeolites [6], mesoporous silica [7], metal organic frameworks (MOFs) [8], and covalent organic frameworks (COFs) [9], have been employed for carbon dioxide capture. However, most of them are associated with several shortcomings, for instance, high costs and complicated synthetic processes, which greatly hinder their industrial implementation. Biochar, a byproduct of biomass pyrolysis, shows great potential as an inexpensive and efficient sorbent for CO₂ capture due to its abundant and renewable feedstock, simple preparation process, wealthy pore structures and functional groups, and high chemical and thermal stability [10–12]. Nowadays, biochar has been extensively used in many fields, such as gas adsorption [13], wastewater decontamination [14], and supercapacitors [15].

Bamboo, as a perennial grass, naturally spreads all over the world (except Europe), and most of them are relatively fast-growing [16,17]. Due to its environmental friendliness,

low price, and renewability, bamboo can be a good feedstock to prepare biochar sorbents for CO₂ capture [18]. However, biochars are commonly obtained via a two-step process, i.e., thermal pyrolysis at first and then being activated using KOH, which leads to an increase in operational difficulty and resource consumption [19]. Particularly, the use of highly corrosive KOH causes safety issues and equipment damage, which also hinders the scale-up and practical application of the conventional pyrolysis techniques. Moreover, the bamboo biochar obtained via conventional pyrolysis is usually associated with the drawbacks of poor surface functionality and a high content of impurities [20].

Recently, salt-assisted pyrolysis, i.e., molten salt pyrolysis, has attracted incremental research interest because of its enhanced heating effect, improved textural and structural properties, and enriched surface oxygen-containing functional groups [21,22]. In this novel pyrolysis process, biomass is carbonized and activated by liquid fused salts to form porous biochars via one-step pyrolyzation, which can not only simplify the preparation procedure but also promote biochar surface functionality. Many efforts have been devoted to biomass pyrolysis in molten salts, however, most of which usually use single K₂CO₃ as the salt media with a high melting point of 899 °C [23], leading to high energy consumption, severe corrosion issues, and inadequate contact between salts and biomass. What is more, the effect of molten salt on the pore properties and surface functional groups of biochars is still controversial. In this work, eutectic salt, i.e., Li₂CO₃ + K₂CO₃, is adopted as the molten salt medium with a melting point of 488 °C [23]. Bamboo biochars are obtained via a simple one-pot carbonization and activation method, i.e., pyrolysis of bamboo powders in eutectic salts (Li₂CO₃ + K₂CO₃) at 500–600 °C in the air. The effects of heating temperature on textural and structural features and carbon dioxide capture performances of bamboo biochars are studied. Moreover, the role of eutectic salt in adjusting the carbon matrix and functional groups of bamboo biochars is addressed as well.

2. Preparation and Characterization of Bamboo Biochars

First, 9.32 g of lithium carbonate (Li₂CO₃) and 10.68 g of potassium carbonate (K₂CO₃) are fully blended. The molar ratio of Li₂CO₃/K₂CO₃ is ca. 0.62:0.32. Then, the salt mixture is put onto 4 g of bamboo powder in a capped crucible and subsequently heated at 500, 550, and 600 °C for 2 h [24]. Finally, bamboo biochars are obtained after washing and drying and are designated as MBC_x (*x* denotes heating temperature). BC600 is acquired using the conventional pyrolyzation method at 600 °C without adding salts. The microstructures and chemical properties of bamboo biochars are examined using a scanning electron microscope (SEM), a Fourier transform infrared (FTIR) and Raman spectrometer, thermogravimetry (TG), and an X-ray photoelectron spectroscope (XPS). N₂ adsorption-desorption isotherms are tested at 77 K. Prior to analysis, biochars are degassed in a vacuum at 120 °C for 6 h. Specific surface areas (SSA) and pore properties are estimated using Brunauer–Emmett–Teller (BET) and Barrett–Joyner–Halenda (BJH) methods using desorption branches, respectively. CO₂ adsorption tests are performed on a physical adsorption apparatus at 1 bar and 25 °C. Prior to adsorption, biochars are degassed at 200 °C for 6 h. The device types and operational details have been fully described elsewhere [25].

3. Results and Discussion

3.1. Physical Properties of Bamboo Biochars

Figure 1 shows the SEM images for different bamboo biochars. MBC500 and MBC600 show flaky structures with curved edges. A few fibrous structures are also observed for MBC550. BC600 is composed of massive stereoporous structures. This implies that salt-assisted pyrolyzation distinctly affects the microstructures of bamboo biochars. Figure 2 shows the energy dispersive spectrometer (EDS) profiles of bamboo biochars. Characteristic signals of carbon and oxygen are observed over all bamboo biochars, suggesting that carbon and oxygen are the major components of all bamboo biochars. Moreover, characteristic signals of potassium and lithium are not detected over MBC_x, indicating that most salts can be washed out after rinsing.

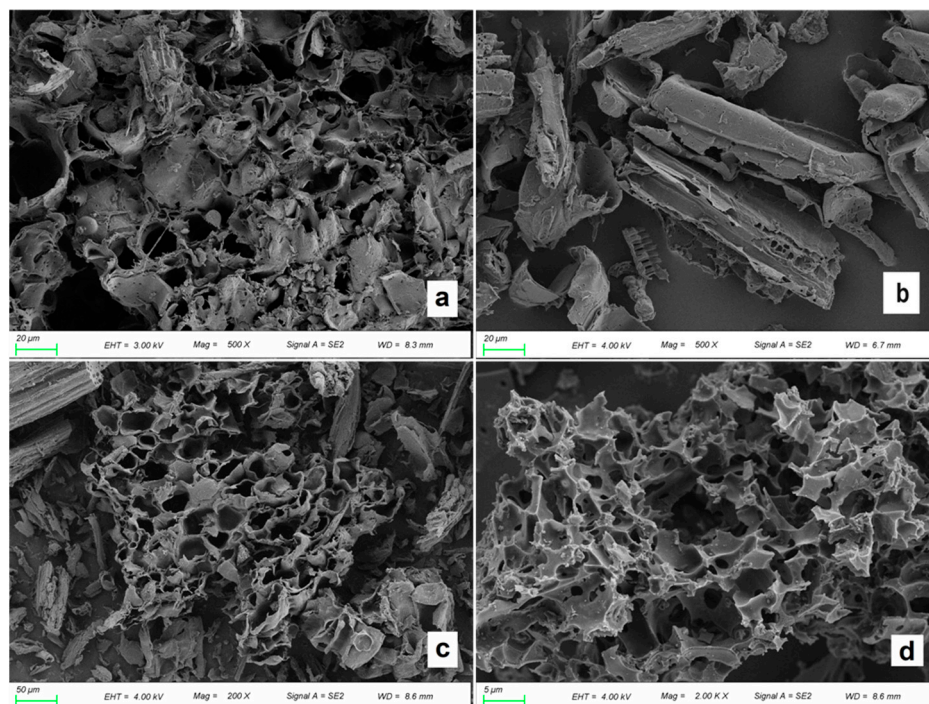


Figure 1. SEM images: (a) MBC500, (b) MBC550, (c) MBC600, and (d) BC600.

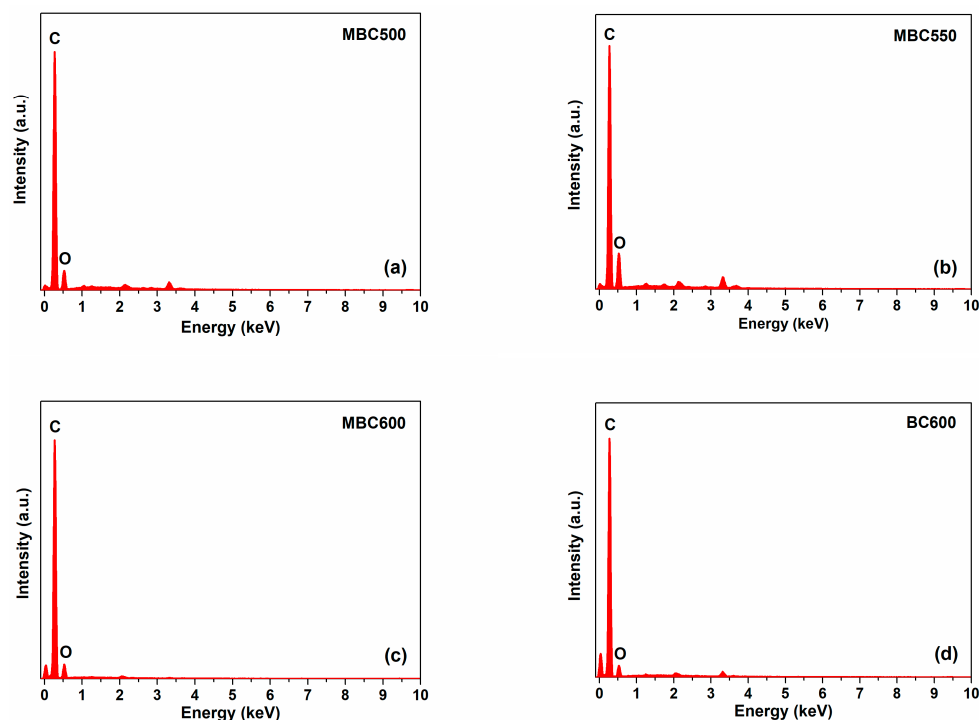


Figure 2. EDS profiles: (a) MBC500, (b) MBC550, (c) MBC600, and (d) BC600.

N₂ physical adsorption isotherms for bamboo biochars are shown in Figure 3, accompanied by textural data in Table 1. N₂ uptakes progressively climb with the elevation of relative pressures for all bamboo biochars, and the desorption branches show hysteresis, suggesting the occurrence of capillary condensation. Furthermore, all sorbents mainly display type IV isotherms, an indication of the existence of massive mesopores [26,27]. As presented in Figure 4, MBC500 shows a bimodal pore size distribution, with pore sizes centered at 3.5 and 7.4 nm. When the pyrolysis temperature elevates to 550–600 °C, bamboo

biochars all show only a sharp peak at 3.9 nm. This indicates that some bigger pores may collapse at elevated pyrolysis temperatures. The textural properties of bamboo biochars are also shown in Table 1. SSA of MBCx first ascends and then descends with the elevation of the heating temperature, which is in the range of 89–109 m²/g. The pore volumes and mean pore sizes of bamboo biochars basically decrease with rising pyrolysis temperatures, which are in the range of 0.180–0.247 cm³/g and 8.0–10.8 nm. BC600 shows the biggest SSA of 113 m²/g and the smallest pore size of 7.1 nm. This indicates that salt-assisted pyrolysis effectively enlarges the pore sizes of bamboo biochars.

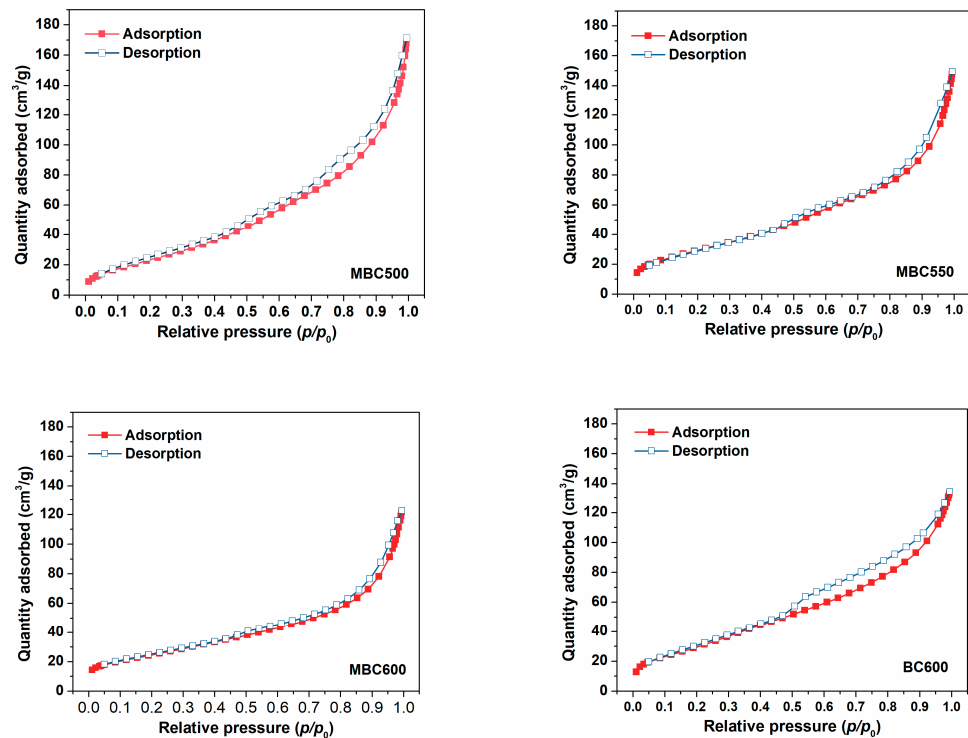


Figure 3. N₂ adsorption-desorption curves for MBC500, MBC550, MBC600, and BC600.

Table 1. Textural properties and Raman and XPS analysis for bamboo biochars.

Samples	SSA (m ² /g)	Pore Volume (cm ³ /g)	Pore Size (nm)	Yield	I _D /I _G	O _α /O _β	CO ₂ Capacity (mmol/g)
MBC500	92	0.247	10.8	12.7%	0.76	0.83	2.06
MBC550	109	0.218	8.0	10.9%	0.77	0.85	2.32
MBC600	89	0.180	8.1	4.5%	1.14	0.98	2.25
BC600	113	0.201	7.1	23.8%	0.75	0.68	1.83

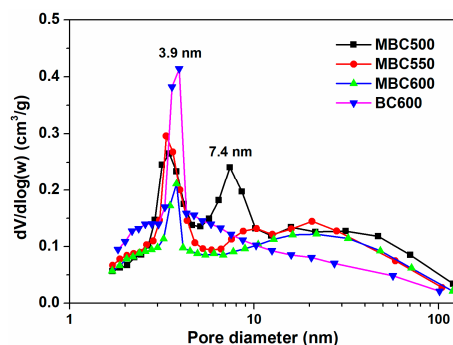


Figure 4. Pore size distribution curves for MBC500, MBC550, MBC600, and BC600.

With the temperature rising from 500 to 550 °C, the mass yield slightly decreases from 12.7 to 10.9 wt%. It reduces over a half to 4.5 wt% when the temperature reaches 600 °C, which is greatly smaller than that of BC600 (23.8 wt%). Molten carbonates provide active CO_3^{2-} anions, which can damage the carbon matrix of bamboo biochars ($2\text{CO}_3^{2-} + 4\text{C} \rightarrow 6\text{CO} + 4\text{e}^-$) [28], leading to the decline of biochar mass yield. Higher pyrolysis temperatures can enhance the activity of carbonate anions and thereby intensify the mass loss of biochars. What is more, the small content of O_2 in the capped crucible likely penetrates into salt melts and reacts with active carbon atoms, converting some carbon atoms into carbon dioxide or carbon monoxide. Higher pyrolysis temperatures can amplify this etching effect, leading to a rapid decrease in product yield at 600 °C.

Raman spectra for bamboo biochars are shown in Figure 5a. Feature signals at 1349 cm^{-1} (D) represent defective and unordered structures, while feature signals at 1588 cm^{-1} (G) denote graphite structures [29]. The I_D/I_G ratio of MBC600 (1.14) significantly surpasses BC600 (0.75). This also implies that molten carbonates can damage the carbon matrix of bamboo biochars when using the salt-assisted pyrolyzation method, resulting in the production of more defects in MBC600. With the pyrolysis temperature rising from 500 to 550 °C, the I_D/I_G ratios slightly increase from 0.76 for MBC500 to 0.77 for MBC550 and greatly rise up to 1.14 for MBC600. Higher pyrolysis temperatures can produce highly active salt ions, which can amplify the etching effect of molten carbonates and thereby create more defects in the carbon frameworks of bamboo biochars [30].

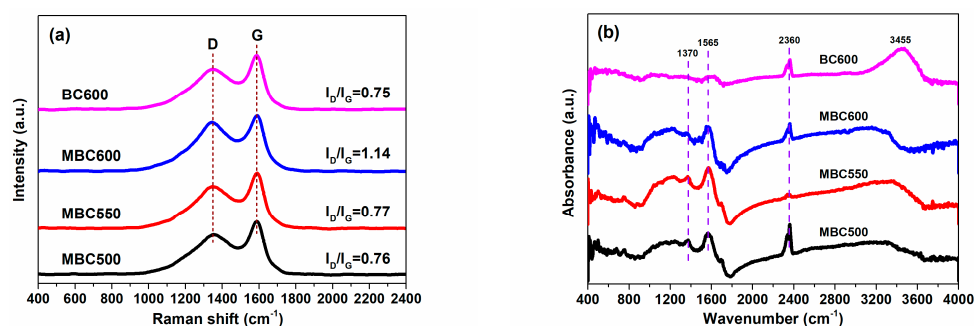


Figure 5. Raman (a) and FTIR (b) spectra for MBC500, MBC550, MBC600, and BC600.

The FTIR spectra for bamboo biochars are shown in Figure 5b. Three intense peaks at 1370 , 1565 , and 2360 cm^{-1} are observed for all biochars, which are ascribed to aliphatic C-H, graphitic C=C, and carbonyl C=O vibrations [22], respectively. A bulge peak at 3455 cm^{-1} is detected for BC600, which is attributed to the vibration of hydroxy (-OH) groups. Elemental compositions for bamboo biochars are shown in Table 2. The dominant components for BC600 are C and O elements with mass percents of 78.13 and 14.52 wt%, respectively. The H/C and O/C molar ratios for BC600 are 0.35 and 0.14, respectively. After molten salt treatment, the carbon content for MBC x significantly reduces to 65.97–67.96 wt%, whereas the oxygen content for MBC x greatly increases to 22.58–29.21 wt%. The H/C and O/C molar ratios for MBC x visibly increase to 0.37–0.46 and 0.25–0.33, respectively. Particularly, the oxygen content and O/C molar ratio for MBC600 are more than doubled as compared with BC600. This indicates that active salt ions can etch the carbon matrix of bamboo biochars, resulting in a decline in carbon contents [31,32]. In addition, the oxygen in carbonates may be incorporated into the carbon matrix of bamboo biochars and thereby increase the oxygen content, which may contribute to the enhanced CO_2 capture ability of MBC x .

Figure 6 shows the TG and DTG profiles of MBC x and BC600. They basically display three decomposing stages. Initial mass loss is less than 10% for MBC x and BC600 within 30–120 °C, which corresponds to the desorption of adsorbates such as H_2O and O_2 . Very little mass decrement is observed in the second stage within 120–350 °C, which likely relates to the decomposition or burning of volatile species in the bamboo biochar. Maximum mass decrement happens from 350 to 500 °C for MBC500, MBC550, and BC600 and from 350 to

550 °C for MBC600 with mass loss of ca. 75–90%, which is plausibly ascribed to degradation or burning of carbon components [33]. From DTG curves, the decomposition temperatures for MBC600 and BC600 are around 474 and 435 °C, respectively. Moreover, BC600 shows a much higher decomposition rate than that of MBCx. These facts indicate that molten salt pyrolysis can improve the thermal stability of the biochar.

Table 2. Elemental compositions of bamboo biochars (wt%).

Samples	C *	H *	O *	N *	Ash *	H/C #	O/C #
MBC500	66.19	2.56	24.82	0.64	5.79	0.46	0.28
MBC550	67.96	2.46	22.58	0.68	6.32	0.43	0.25
MBC600	65.97	2.05	29.21	0.67	2.10	0.37	0.33
BC600	78.13	2.28	14.52	0.55	4.52	0.35	0.14

Note: * dry basis, # molar ratio.

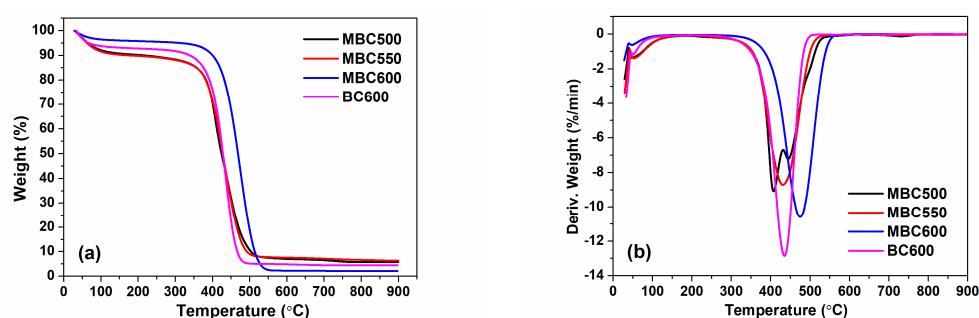


Figure 6. TG (a) and DTG (b) curves for MBC500, MBC550, MBC600, and BC600 (performed in an air atmosphere with a heating rate of 10 °C/min).

The ash content of MBC600 (2.10 wt%) is greatly inferior to BC600 (4.52 wt%), which infers that carbonate melt dissolves a portion of the ash species of bamboo biochar [34]. In addition, with the temperature rising from 550 to 600 °C, the carbon and ash contents of biochars both reduce. On the one hand, higher temperatures can enhance the etching effect of salt ions, resulting in a decrease in carbon content. On the other hand, higher temperatures can also enhance the dissolving capacity of salt ions with respect to ash components and thereby reduce the ash content.

3.2. Chemical Properties of Bamboo Biochars

Figures 7 and 8 show electron densities and valence bonding of carbon and oxygen atoms on the bamboo biochar surface. With respect to C 1s profiles, peaks located at 284.0–284.5 eV vest in aromatic carbon (C_{α} , C=C), and peaks located at 285.5–285.8 eV correspond to the C atoms bonded to hydroxyl groups (C_{β} , C-O-H) [35,36]. With respect to O 1s profiles, peaks located at 531.2–531.8 eV relate to active oxygen (O_{α} , C=O) [37], while peaks located at 533.0–533.2 eV are assigned to oxygen in hydroxy groups (O_{β} , -OH) [38]. As shown in Table 1, the O_{α}/O_{β} proportion for BC600 is only 0.68, an indication of the trace content of active oxygen existing on BC600. With temperatures rising from 500 to 600 °C, the O_{α}/O_{β} proportions for MBCx gradually increase from 0.83 to 0.98. This implies that salt-assisted pyrolyzation distinctly augments the content of active oxygen on bamboo biochar surfaces. A part of the oxygen in the capped crucible likely dissolves in salt melts, which is then captured and activated on bamboo biochars during salt-assisted pyrolyzation processes, resulting in the generation of ample active oxygen on MBCx. Moreover, the oxygen atoms in carbonates may also react with the carbon atoms in bamboo biochars to form C=O bonds, which leads to an increase in chemisorbed oxygen.

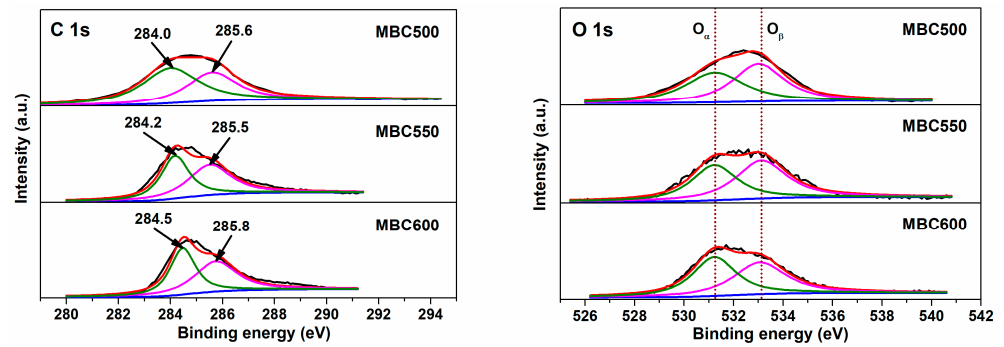


Figure 7. XPS profiles for MBC500, MBC550, and MBC600.

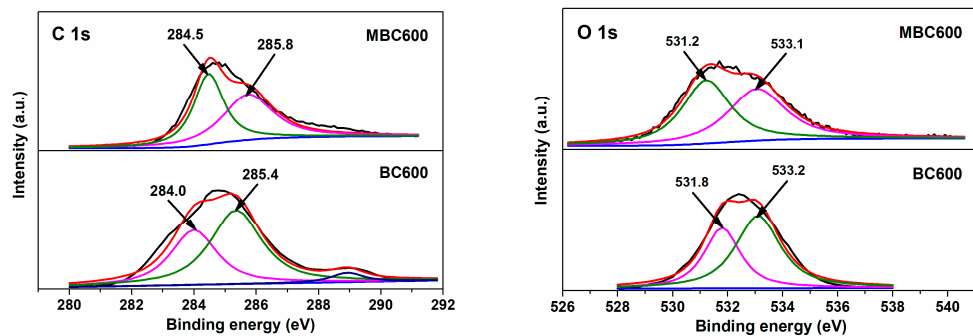


Figure 8. XPS profiles for MBC600 and BC600.

3.3. Carbon Dioxide Adsorption

Carbon dioxide adsorption curves for MBCx and BC600 at 25 °C and 100 kPa are shown in Figure 9 and Table 1. BC600 shows the smallest carbon dioxide capacity of 1.83 mmol/g, likely due to the lowest contents of defects and active oxygen. After molten salt activation, the CO₂ uptakes for MBCx significantly increase to 2.06–2.32 mmol/g, which is plausibly owing to the increased defects in the carbon matrix and chemisorbed oxygen contents. This indicates that salt-assisted pyrolyzation effectively promotes the activity of bamboo biochars with respect to carbon dioxide capture. On the one hand, the electropositive C atom in carbon dioxide could adsorb the electronegative O atom (i.e., C=O) of bamboo biochars via Lewis acid-base interaction, which plausibly contributes to enhanced CO₂ uptake [39]. On the other hand, carbon defects can function as electron receptors [40] which pull electrons from the O atom of carbon dioxide via polarization, which results in augmented carbon dioxide capture. What is more, the specific surface area of BC600 surpasses that of MBCx, however, it displays the worst carbon dioxide capture. This implies that physical properties may show an insignificant impact on the carbon dioxide adsorption capabilities of bamboo biochars, whereas chemical properties, for instance, active oxygen and defective structures, show prominent influences on the carbon dioxide adsorption capabilities of bamboo biochars. As shown in Table 3, the CO₂ uptake of MBC550 is bigger than or comparable to some biochars [41–43].

Table 3. CO₂ uptakes of different sorbents at 25 °C and 1 bar.

Sorbents	Precursors	SSA (m ² /g)	Adsorption Conditions	CO ₂ Uptakes (mmol/g)	Ref.
MBC550	bamboo	109	25 °C (1 bar)	2.32	this work
CSAC	chestnut shell	1254	25 °C (1 bar)	1.70	[41]
WSAC	walnut shell	1489	25 °C (1 bar)	2.10	[41]
MSAC	macadamia shell	1151	25 °C (1 bar)	1.97	[41]
AC	peat	942	25 °C (1 bar)	2.46	[42]
AC	white wood	1400	25 °C (1 bar)	1.80	[43]

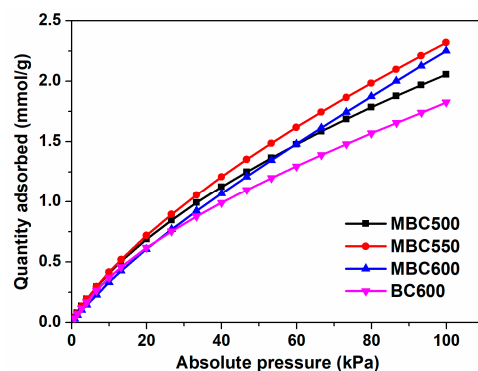


Figure 9. CO₂ adsorption isotherms at 25 °C for MBC500, MBC550, MBC600, and BC600.

4. Conclusions

Middle-temperature eutectic salts (Li₂CO₃ + K₂CO₃) are adopted as the molten salt media to prepare bamboo biochars for the sake of enhancing heat transfer and lowering energy consumption. Salt-assisted pyrolyzation greatly promotes the surface functionality of bamboo biochars to produce ample active oxygen and defective structures, thereby enhancing the carbon dioxide capture ability of bamboo biochars. The rise in heating temperature progressively increases the defect structure of bamboo biochar. MBC550 presents an optimal CO₂ uptake of 2.32 mmol/g at 25 °C and 1 bar, which distinctly surpasses that of conventional bamboo biochar (1.83 mmol/g) prepared via pyrolysis in an inert atmosphere without adding salts. Molten salt pyrolysis can impart bamboo biochars with better thermal stability, higher oxygen contents, and more carbon defects, thereby enhancing their CO₂ capture activities.

Author Contributions: Conceptualization, D.L. (Dongjing Liu) and B.L.; methodology, X.X. and D.L. (Dongjing Liu); validation, X.X. and M.L.; formal analysis, D.L. (Dan Lin); investigation, X.X. and D.L. (Dan Lin); resources, C.L. and B.L.; data curation, X.X. and M.L.; writing—original draft preparation, D.L. (Dan Lin); writing—review and editing, D.L. (Dongjing Liu); funding acquisition, B.L. and D.L. (Dongjing Liu) All authors have read and agreed to the published version of the manuscript.

Funding: This study is supported by the National Natural Science Foundation of China (52276196, 51876225), the High-Level Talent Foundation of Anhui Agricultural University (rc412307), and the Senior Talent Foundation of Jiangsu University (grant no. 18JDG017).

Data Availability Statement: Data will be made available on request.

Conflicts of Interest: The authors declare no conflict of interest.

References

- Satterthwaite, D. Cities' contribution to global warming: Notes on the allocation of greenhouse gas emissions. *Environ. Urban.* **2008**, *20*, 539–549. [[CrossRef](#)]
- Bhave, A.; Taylor, R.H.; Fennell, P.; Livingston, W.R.; Shah, N.; Mac Dowell, N.; Dennis, J.; Kraft, M.; Pourkashanian, M.; Insa, M. Screening and techno-economic assessment of biomass-based power generation with CCS technologies to meet 2050 CO₂ targets. *Appl. Energy* **2017**, *190*, 481–489. [[CrossRef](#)]
- Rochelle, G.T. Amine scrubbing for CO₂ capture. *Science* **2009**, *325*, 1652–1654. [[CrossRef](#)] [[PubMed](#)]
- Algozeeb, W.A.; Savas, P.E.; Yuan, Z.; Wang, Z.; Kittrell, C.; Hall, J.N.; Chen, W.; Bollini, P.; Tour, J.M. Plastic waste product captures carbon dioxide in nanometer pores. *ACS Nano* **2022**, *16*, 7284–7290. [[CrossRef](#)] [[PubMed](#)]
- Lee, S.Y.; Park, S.J. A review on solid adsorbents for carbon dioxide capture. *J. Ind. Eng. Chem.* **2015**, *23*, 1–11. [[CrossRef](#)]
- Kumar, S.; Srivastava, R.; Koh, J. Utilization of zeolites as CO₂ capturing agents: Advances and future perspectives. *J. CO₂ Util.* **2020**, *41*, 101251. [[CrossRef](#)]
- Xu, X.; Song, C.; Andresen, J.M.; Miller, B.G.; Scaroni, A.W. Novel Polyethylenimine-modified mesoporous molecular sieve of MCM-41 type as high-capacity adsorbent for CO₂ capture. *Energy Fuels* **2002**, *16*, 1463–1469. [[CrossRef](#)]
- Zhao, M.; Yang, Y.; Gu, X. MOF based CO₂ capture: Adsorption and membrane separation. *Inorg. Chem. Commun.* **2023**, *152*, 110722. [[CrossRef](#)]
- Liu, X.; Lim, G.J.H.; Wang, Y.; Zhang, L.; Mullangi, D.; Wu, Y.; Zhao, D.; Ding, J.; Cheetham, A.K.; Wang, J. Binder-free 3D printing of covalent organic framework (COF) monoliths for CO₂ adsorption. *Chem. Eng. J.* **2021**, *403*, 126333. [[CrossRef](#)]

10. Quan, C.; Zhou, Y.; Wang, J.; Wu, C.; Gao, N.B. Biomass-based carbon materials for CO₂ capture: A review. *J. CO₂ Util.* **2023**, *68*, 102373. [[CrossRef](#)]
11. Shen, Y.F. Preparation of renewable porous carbons for CO₂ capture-A review. *Fuel Process. Technol.* **2022**, *236*, 107437. [[CrossRef](#)]
12. Chatterjee, R.; Sajjadi, B.; Mattern, D.L.; Chen, W.; Zubatiuk, T.; Leszczynska, D.; Leszczynski, J.; Egiebor, N.O.; Hammer, N. Ultrasound cavitation intensified amine functionalization: A feasible strategy for enhancing CO₂ capture capacity of biochar. *Fuel* **2018**, *225*, 287–298. [[CrossRef](#)]
13. Wen, C.; Liu, T.; Wang, D.; Wang, Y.; Chen, H.P.; Luo, G.Q.; Zou, Z.J.; Li, C.; Xu, M.H. Biochar as the effective adsorbent to combustion gaseous pollutants: Preparation, activation, functionalization and the adsorption mechanisms. *Prog. Energy Combust.* **2023**, *99*, 101098. [[CrossRef](#)]
14. Alalwan, H.A.; Alminshid, A.H.; Mohammed, M.M.; Mohammed, M.F.; Shadhar, M.H. Reviewing of using nanomaterials for wastewater treatment. *Pollution* **2022**, *8*, 995–1013.
15. Yang, L.; Qiu, J.; Wang, Y.; Guo, S.; Feng, Y.; Dong, D.; Yao, J. Molten salt synthesis of hierarchical porous carbon from wood sawdust for supercapacitors. *J. Electroanal. Chem.* **2020**, *856*, 113673. [[CrossRef](#)]
16. Siddiqui, N.; Don, J.; Mondal, K.; Mahajan, A. Development of bamboo-derived sorbents for mercury removal in gas phase. *Environ. Technol.* **2011**, *32*, 383–394. [[CrossRef](#)]
17. Cheng, L.; Adhikari, S.; Wang, Z.; Ding, Y. Characterization of bamboo species at different ages and bio-oil production. *J. Anal. Appl. Pyrol.* **2015**, *116*, 215–222. [[CrossRef](#)]
18. Tan, Z.; Xiang, J.; Su, S.; Zeng, H.; Zhou, C.; Sun, L.S.; Hu, S.; Qiu, J. Enhanced capture of elemental mercury by bamboo-based sorbents. *J. Hazard. Mater.* **2012**, *239*, 160–166. [[CrossRef](#)]
19. Goel, C.; Mohan, S.; Dinesha, P. CO₂ capture by adsorption on biomass-derived activated char: A review. *Sci. Total Environ.* **2021**, *798*, 149296. [[CrossRef](#)]
20. Zhu, X.; Sun, M.; Zhu, X.; Guo, W.; Luo, Z.; Cai, W.; Zhu, X. Molten salt shielded pyrolysis of biomass waste: Development of hierarchical biochar, salt recovery, CO₂ adsorption. *Fuel* **2023**, *334*, 126565. [[CrossRef](#)]
21. Diez, N.; Fuertes, A.B.; Sevilla, M. Molten salt strategies towards carbon materials for energy storage and conversion. *Energy Storage Mater.* **2021**, *38*, 50–69. [[CrossRef](#)]
22. Li, B.; Tang, J.Z.; Xie, X.; Wei, J.T.; Xu, D.; Shi, L.; Ding, K.; Zhang, S.; Hu, X.; Zhang, S.; et al. Char structure evolution during molten salt pyrolysis of biomass: Effect of temperature. *Fuel* **2023**, *331*, 125747. [[CrossRef](#)]
23. Huang, L.; Hu, Z.; Jin, H.; Wu, J.; Liu, K.; Xu, Z.; Wan, J.; Zhou, H.; Duan, J.; Hu, B.; et al. Salt-assisted synthesis of 2D materials. *Adv. Funct. Mater.* **2020**, *30*, 1908486. [[CrossRef](#)]
24. Liu, D.J.; Yang, L.T.; Wu, J.; Li, B. Molten salt shielded preparation of rice straw biochars doped by copper sulfide for elemental mercury capture. *J. Energy Inst.* **2022**, *102*, 176–183. [[CrossRef](#)]
25. Li, B.; Li, M.; Xie, X.; Li, C.E.; Liu, D.J. Pyrolysis of rice husk in molten lithium chloride: Biochar structure evolution and CO₂ adsorption. *J. Energy Inst.* **2024**, *113*, 101526. [[CrossRef](#)]
26. Oh, Y.; Morris, C.D.; Kanatzidis, M.G. Polysulfide chalcogels with ion-exchange properties and highly efficient mercury vapor sorption. *J. Am. Chem. Soc.* **2012**, *134*, 14604–14608. [[CrossRef](#)] [[PubMed](#)]
27. López, R.H.; Vidales, A.M.; Zgrablich, G. Percolation effects on adsorption-desorption hysteresis. *Langmuir* **2000**, *16*, 6999–7005. [[CrossRef](#)]
28. McKee, D.W. Mechanisms of the alkali metal catalysed gasification of carbon. *Fuel* **1983**, *62*, 170–175. [[CrossRef](#)]
29. Lyon, L.A.; Keating, C.D.; Fox, A.P.; Baker, B.E.; He, L.; Nicewarner, S.R.; Mulvaney, S.P.; Natan, M.J. Raman spectroscopy. *Anal. Chem.* **1998**, *70*, 341–362. [[CrossRef](#)]
30. Yan, S.; Lin, J.; Liu, P.; Zhao, Z.; Lian, J.; Chang, W.; Yao, L.; Liu, Y.; Lin, H.; Han, S. Preparation of nitrogen-doped porous carbons for high-performance supercapacitor using biomass of waste lotus stems. *RSC Adv.* **2018**, *8*, 6806–6813. [[CrossRef](#)]
31. Wang, C.; Wu, D.; Wang, H.; Gao, Z.; Xu, F.; Jiang, K. Nitrogen-doped two-dimensional porous carbon sheets derived from clover biomass for high performance supercapacitors. *J. Power Sources* **2017**, *363*, 375–383. [[CrossRef](#)]
32. Liu, X.; Antonietti, M. Molten salt activation for synthesis of porous carbon nanostructures and carbon sheets. *Carbon* **2014**, *69*, 460–466. [[CrossRef](#)]
33. Kamran, U.; Park, S.J. Tuning ratios of KOH and NaOH on acetic acid-mediated chitosan-based porous carbons for improving their textural features and CO₂ uptakes. *J. CO₂ Util.* **2020**, *40*, 101212. [[CrossRef](#)]
34. Shen, J.; Hu, H.Y.; Xu, M.; Liu, H.; Xu, K.; Zhang, X.; Yao, H.; Naruse, I. Interactions between molten salts and ash components during Zhundong coal gasification in eutectic carbonates. *Fuel* **2017**, *207*, 365–372. [[CrossRef](#)]
35. Stankovich, S.; Dikin, D.A.; Piner, R.D.; Kohlhaas, K.A.; Kleinhammes, A.; Jia, Y.; Wu, Y.; Nguyen, S.B.T.; Ruoff, R.S. Synthesis of graphene-based nanosheets via chemical reduction of exfoliated graphite oxide. *Carbon* **2007**, *45*, 1558–1565. [[CrossRef](#)]
36. Ganguly, A.; Sharma, S.; Papakonstantinou, P.; Hamilton, J. Probing the thermal deoxygenation of graphene oxide using high-resolution in situ X-ray-based spectroscopies. *J. Phys. Chem. C* **2011**, *115*, 17009–17019. [[CrossRef](#)]
37. Akhavan, O. The effect of heat treatment on formation of graphene thin films from graphene oxide nanosheets. *Carbon* **2010**, *48*, 509–519. [[CrossRef](#)]
38. Jampaiah, D.; Ippolito, S.J.; Sabri, Y.M.; Tardio, J.; Selvakannan, P.R.; Nafady, A.; Reddy, B.M.; Bhargava, S.K. Ceria-zirconia modified MnO_x catalysts for gaseous elemental mercury oxidation and adsorption. *Catal. Sci. Technol.* **2016**, *6*, 1792–1803. [[CrossRef](#)]

39. Ma, X.; Yang, Y.; Wu, Q.; Liu, B.; Li, D.; Chen, R.; Wang, C.; Li, H.; Zeng, Z.; Li, L. Underlying mechanism of CO₂ uptake onto biomass-based porous carbons: Do adsorbents capture CO₂ chiefly through narrow micropores? *Fuel* **2020**, *282*, 118727. [[CrossRef](#)]
40. Liu, D.J.; Yang, L.T.; Wu, J.; Li, B. Tuning sulfur vacancies in CoS₂ via a molten salt approach for promoted mercury vapor adsorption. *Chem. Eng. J.* **2022**, *450*, 137956. [[CrossRef](#)]
41. Pu, Q.; Zou, J.; Wang, J.; Lu, S.; Ning, P.; Huang, L.; Wang, Q. Systematic study of dynamic CO₂ adsorption on activated carbons derived from different biomass. *J. Alloy Compd.* **2021**, *887*, 161406. [[CrossRef](#)]
42. García, S.; Gil, M.V.; Martín, C.F.; Pis, J.J.; Rubiera, F.; Pevida, C. Breakthrough adsorption study of a commercial activated carbon for pre-combustion CO₂ capture. *Chem. Eng. J.* **2011**, *171*, 549–556. [[CrossRef](#)]
43. Shahkarami, S.; Azargohar, R.; Dalai, A.K.; Soltan, J. Breakthrough CO₂ adsorption in bio-based activated carbons. *J. Environ. Sci.* **2015**, *34*, 68–76. [[CrossRef](#)] [[PubMed](#)]

Disclaimer/Publisher’s Note: The statements, opinions and data contained in all publications are solely those of the individual author(s) and contributor(s) and not of MDPI and/or the editor(s). MDPI and/or the editor(s) disclaim responsibility for any injury to people or property resulting from any ideas, methods, instructions or products referred to in the content.